Exploiting Zn and Zr synergy in co-doped $Sr(Fe_{1-x}Mo_x)O_{3-\delta}$ – versatile Co-free electrode materials for Solid Oxide Fuel Cells

Margarita Nowakowska[a], Juliusz Dąbrowa[a,], Marek Zajusz[a], Jan Adamczyk[a], Katarzyna Berent[b], Rotraut Merkle[c], Grzegorz Gazdowicz[d], Konrad Świerczek[e,f]*

[a]AGH University of Krakow, Faculty of Materials Science and Ceramics,

Al. Mickiewicza 30, 30-059 Krakow, Poland

[b]AGH University of Krakow, Academic Centre for Materials and Nanotechnology, Al. Mickiewicza 30, 30-059 Krakow, Poland

[c]Max Planck Institute for Solid State Research, Heisenbergstraße 1, Stuttgart, DE-70569, Germany

[d]SOLARIS National Synchrotron Radiation Centre, Jagiellonian University, ul. Czerwone Maki 98, 30-392 Kraków, Poland

[e]AGH University of Krakow, Faculty of Energy and Fuels,

Al. Mickiewicza 30, 30-059 Krakow, Poland

[f]AGH Centre of Energy, AGH University of Krakow,

ul. Czarnowiejska 36, 30-054 Krakow, Poland

* - *corresponding author: dabrowa@agh.edu.pl*

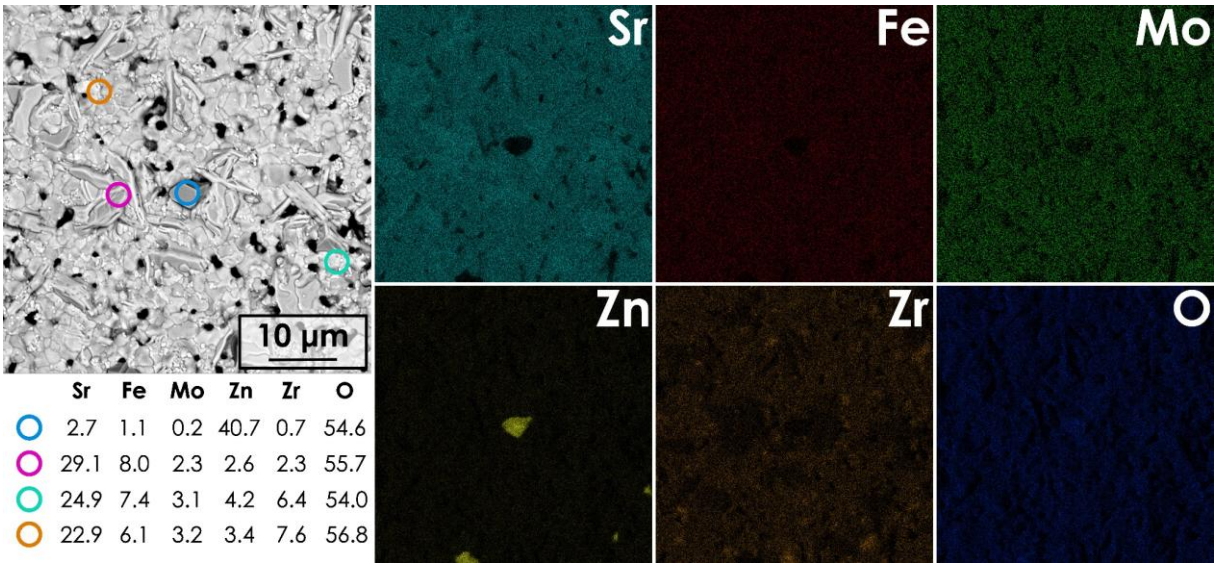

	Sr	Fe	Mo	Zn	Zr	O
○	2.7	1.1	0.2	40.7	0.7	54.6
○	29.1	8.0	2.3	2.6	2.3	55.7
○	24.9	7.4	3.1	4.2	6.4	54.0
○	22.9	6.1	3.2	3.4	7.6	56.8

Figure S1. SEM micrograph and the corresponding results of EDS mapping and point analysis for the $SrFe_{0.375}Mo_{0.125}Zn_{0.25}Zr_{0.25}O_{3-\delta}$ pellet sintered at 1200 °C for 20 h.

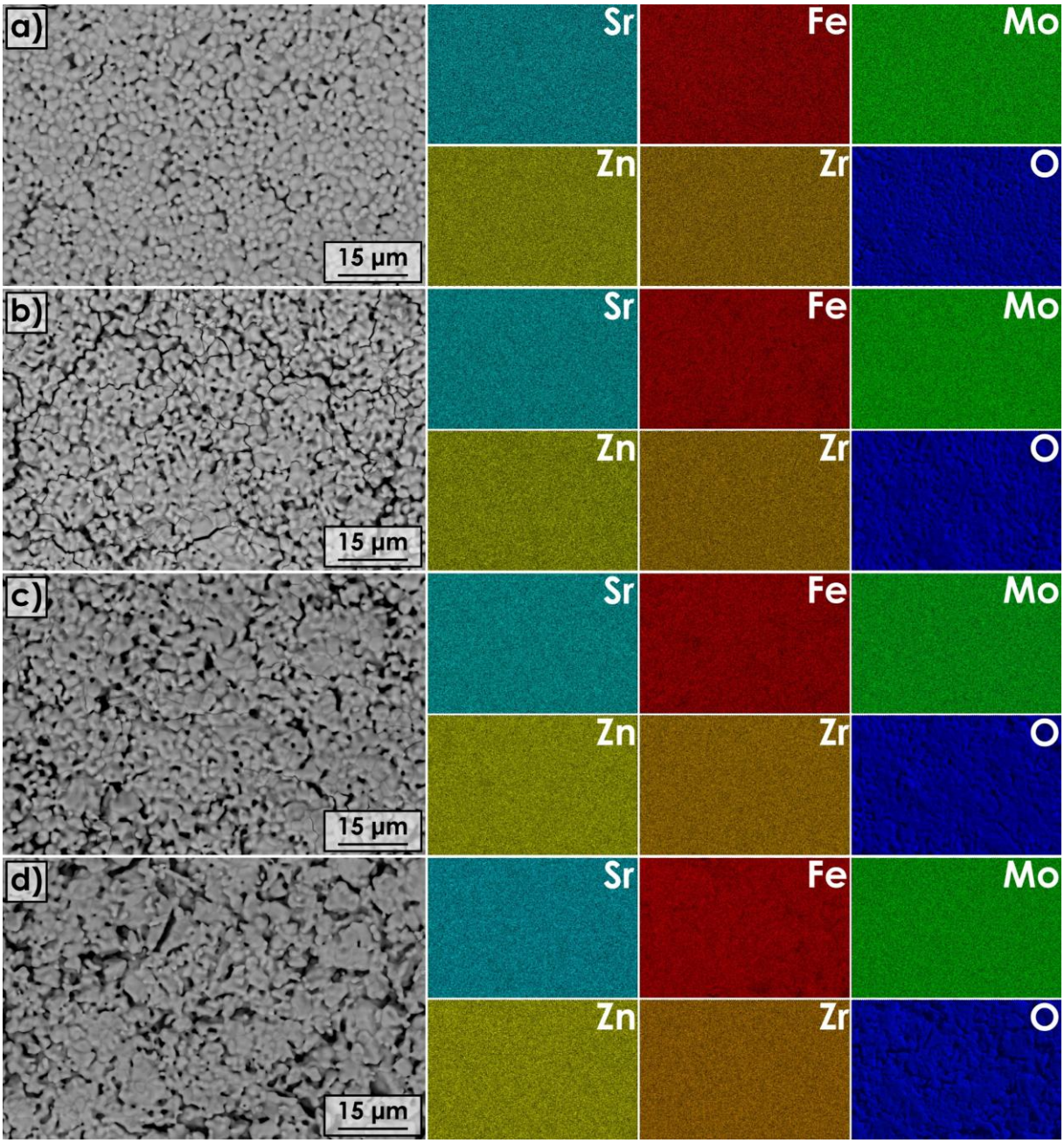

Figure S2. SEM micrograph and the corresponding results of EDS mapping for pellets sintered at 1200 °C for 20 h: a) $SrFe_{0.675}Mo_{0.225}Zn_{0.05}Zr_{0.05}O_{3-\delta}$; b) $SrFe_{0.6}Mo_{0.2}Zn_{0.1}Zr_{0.1}O_{3-\delta}$; c) $SrFe_{0.525}Mo_{0.175}Zn_{0.15}Zr_{0.15}O_{3-\delta}$; d) $SrFe_{0.45}Mo_{0.15}Zn_{0.2}Zr_{0.2}O_{3-\delta}$.

Table S1. The summary of the EDS area analyses for $Sr(Fe_{0.75}Mo_{0.25})_{1-2x}Zn_xZr_xO_{3-\delta}$ (x = 0.05, 0.1, 0.15, and 0.2) materials.

Composition	**[At. %]**					
	Sr	Fe	Mo	Zn	Zr	O
$SrFe_{0.675}Mo_{0.225}Zn_{0.05}Zr_{0.05}O_{3-\delta}$	20.0	16.0	4.5	0.7	1.1	57.7
$SrFe_{0.6}Mo_{0.2}Zn_{0.1}Zr_{0.1}O_{3-\delta}$	19.8	14.6	3.8	1.6	2.1	58.1
$SrFe_{0.525}Mo_{0.175}Zn_{0.15}Zr_{0.15}O_{3-\delta}$	19.6	12.2	3.6	2.5	3.2	58.9
$SrFe_{0.45}Mo_{0.15}Zn_{0.2}Zr_{0.2}O_{3-\delta}$	19.9	11.9	3.1	3.1	4.7	57.3
Composition	**B site cation ratios**					
	Sr	Fe	Mo	Zn	Zr	O
$SrFe_{0.675}Mo_{0.225}Zn_{0.05}Zr_{0.05}O_{3-\delta}$		0.717	0.202	0.031	0.049	
$SrFe_{0.6}Mo_{0.2}Zn_{0.1}Zr_{0.1}O_{3-\delta}$		0.661	0.172	0.072	0.095	
$SrFe_{0.525}Mo_{0.175}Zn_{0.15}Zr_{0.15}O_{3-\delta}$		0.567	0.167	0.116	0.149	
$SrFe_{0.45}Mo_{0.15}Zn_{0.2}Zr_{0.2}O_{3-\delta}$		0.522	0.136	0.136	0.206	

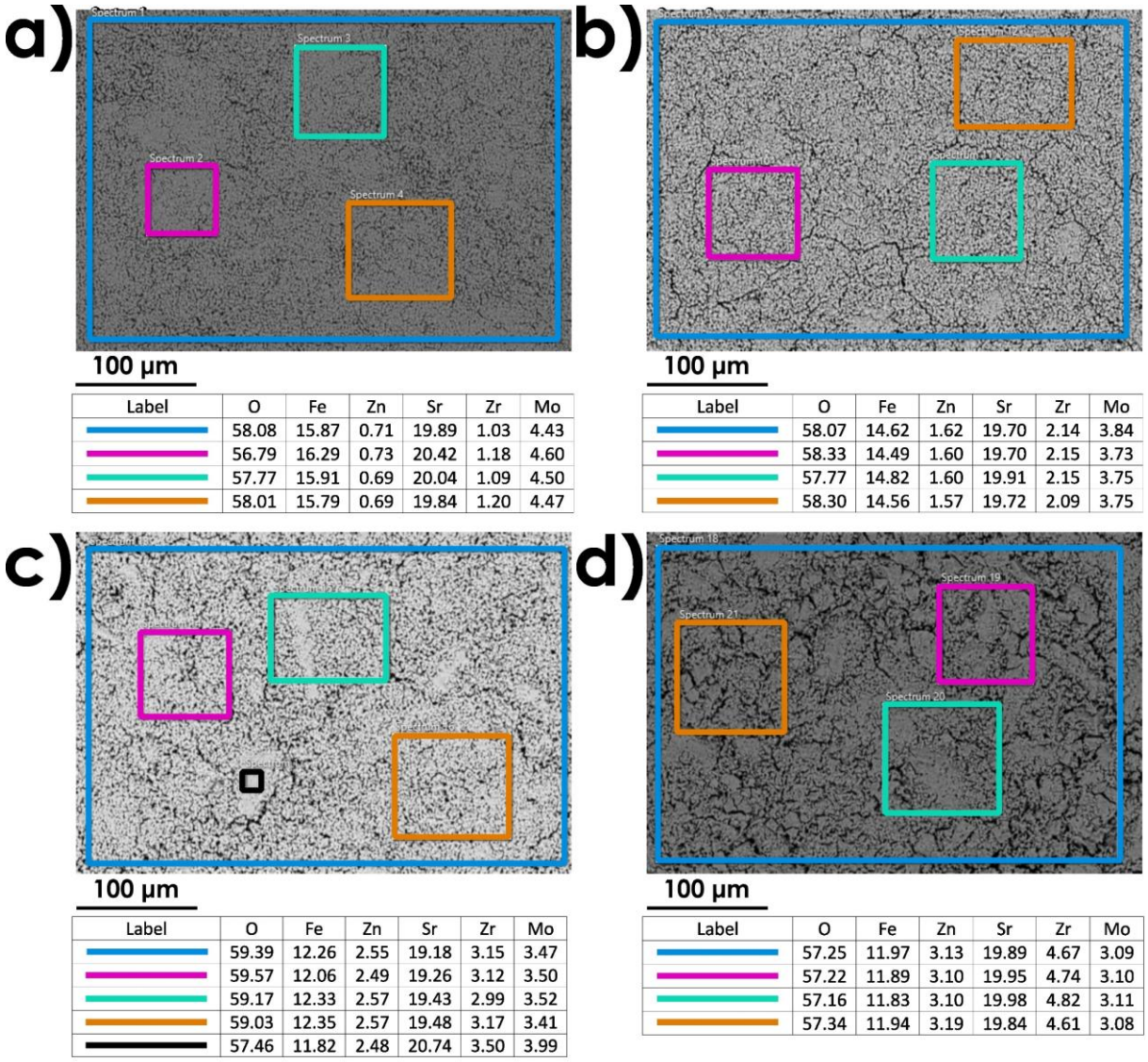

Label	O	Fe	Zn	Sr	Zr	Mo
	58.08	15.87	0.71	19.89	1.03	4.43
	56.79	16.29	0.73	20.42	1.18	4.60
	57.77	15.91	0.69	20.04	1.09	4.50
	58.01	15.79	0.69	19.84	1.20	4.47

Label	O	Fe	Zn	Sr	Zr	Mo
	58.07	14.62	1.62	19.70	2.14	3.84
	58.33	14.49	1.60	19.70	2.15	3.73
	57.77	14.82	1.60	19.91	2.15	3.75
	58.30	14.56	1.57	19.72	2.09	3.75

Label	O	Fe	Zn	Sr	Zr	Mo
	59.39	12.26	2.55	19.18	3.15	3.47
	59.57	12.06	2.49	19.26	3.12	3.50
	59.17	12.33	2.57	19.43	2.99	3.52
	59.03	12.35	2.57	19.48	3.17	3.41
	57.46	11.82	2.48	20.74	3.50	3.99

Label	O	Fe	Zn	Sr	Zr	Mo
	57.25	11.97	3.13	19.89	4.67	3.09
	57.22	11.89	3.10	19.95	4.74	3.10
	57.16	11.83	3.10	19.98	4.82	3.11
	57.34	11.94	3.19	19.84	4.61	3.08

Figure S3. EDS analysis for: a) $SrFe_{0.675}Mo_{0.225}Zn_{0.05}Zr_{0.05}O_{3-\delta}$; b) $SrFe_{0.6}Mo_{0.2}Zn_{0.1}Zr_{0.1}O_{3-\delta}$; c) $SrFe_{0.525}Mo_{0.175}Zn_{0.15}Zr_{0.15}O_{3-\delta}$; d) $SrFe_{0.45}Mo_{0.15}Zn_{0.2}Zr_{0.2}O_{3-\delta}$.

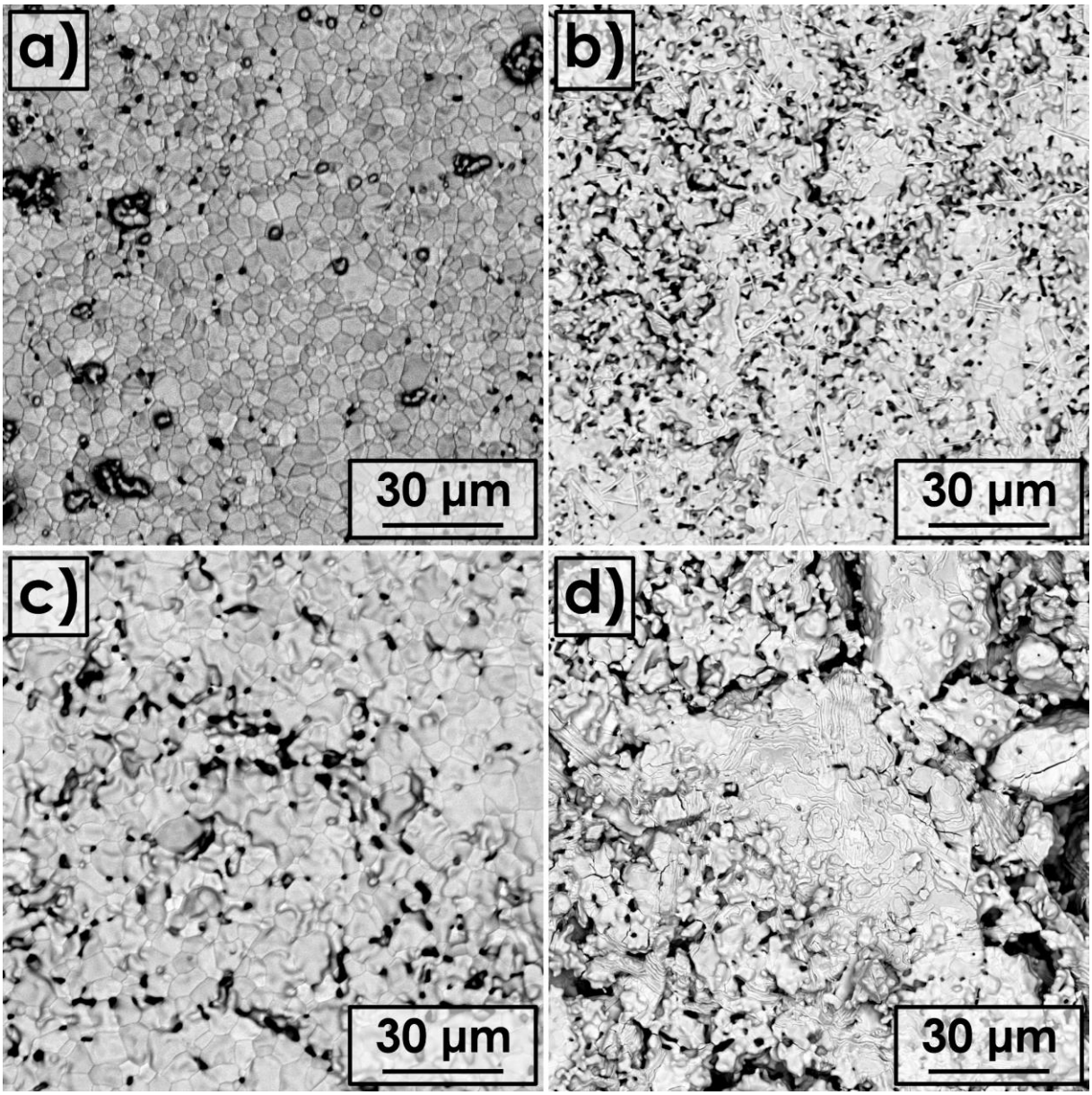

Figure S4. SEM micrographs for dense pellets of: a) $SrFe_{0.675}Mo_{0.225}Zn_{0.05}Zr_{0.05}O_{3-\delta}$ (1300 °C); b) $SrFe_{0.6}Mo_{0.2}Zn_{0.1}Zr_{0.1}O_{3-\delta}$ (1300 °C); c) $SrFe_{0.525}Mo_{0.175}Zn_{0.15}Zr_{0.15}O_{3-\delta}$ (1300 °C); d) $SrFe_{0.45}Mo_{0.15}Zn_{0.2}Zr_{0.2}O_{3-\delta}$ (1250 °C).

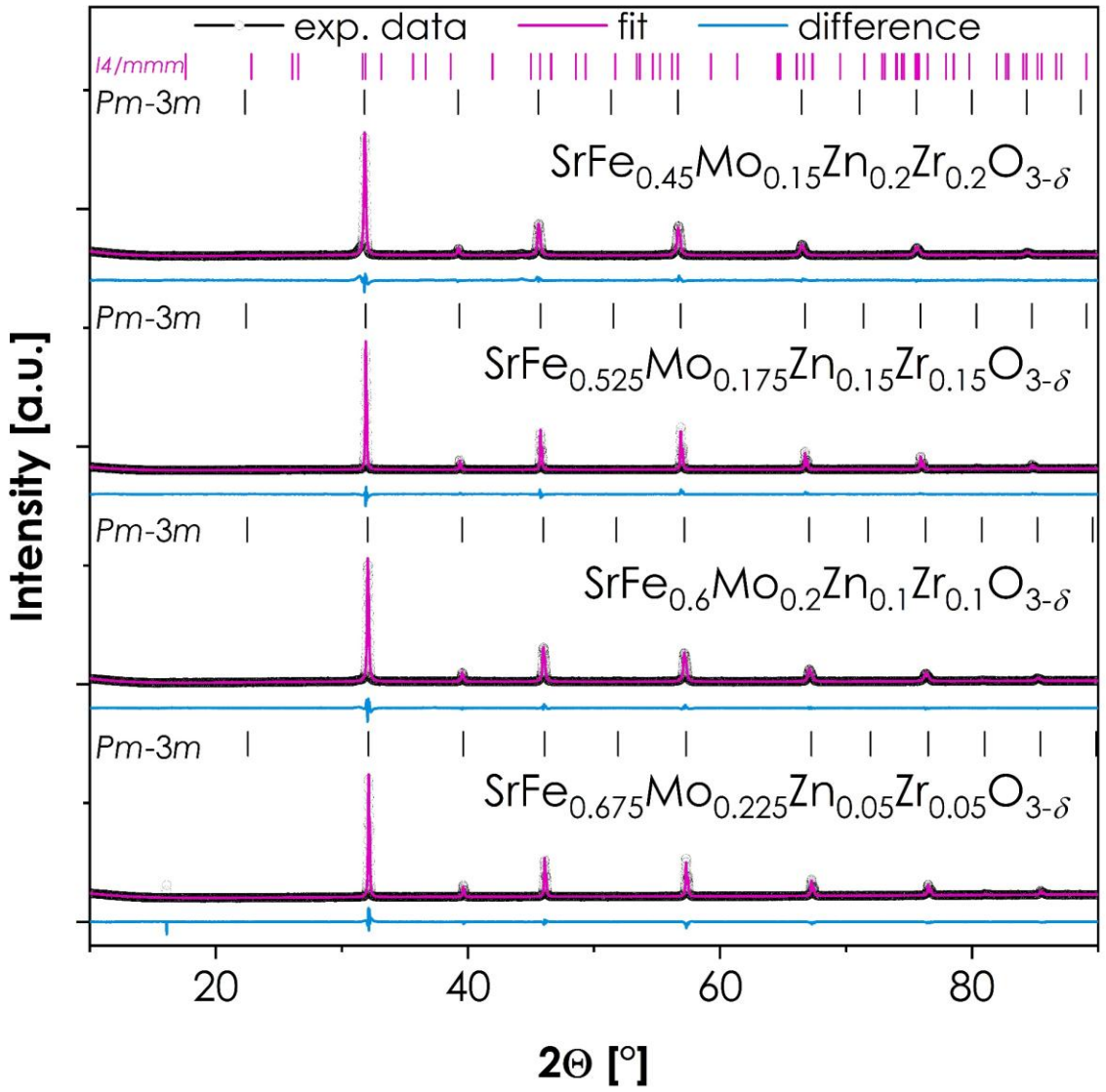

Figure S5. X-ray diffractograms for dense pellets of: a) $SrFe_{0.675}Mo_{0.225}Zn_{0.05}Zr_{0.05}O_{3-\delta}$ (1300 °C); b) $SrFe_{0.6}Mo_{0.2}Zn_{0.1}Zr_{0.1}O_{3-\delta}$ (1300 °C); c) $SrFe_{0.525}Mo_{0.175}Zn_{0.15}Zr_{0.15}O_{3-\delta}$ (1300 °C); d) $SrFe_{0.45}Mo_{0.15}Zn_{0.2}Zr_{0.2}O_{3-\delta}$ (1250 °C). Due to the small content of the second phase, its presence was considered to have negligible effect on the electrical and thermomechanical properties, and sinters from this temperature were used in further studies.

Table S2. The results of Rietveld refinement for $Sr(Fe_{0.75}Mo_{0.25})_{1-2x}Zn_xZr_xO_{3-\delta}$ (x = 0, 0.05, 0.1, 0.15, and 0.2) dense pellets' materials, together with the procedure's residuals.

Composition	Space group	Content [wt.%]	*a* [Å]	c [Å]	*V* [Å^3]	ρ_{the} [g·cm^{-3}]	GoF [-]	Rwp [%]
$SrFe_{0.675}Mo_{0.225}Zn_{0.05}Zr_{0.05}O_{3-\delta}$	*Pm-3m*	100	3.9321(1)	-	60.795(2)	5.5373	2.47	3.61
$SrFe_{0.6}Mo_{0.2}Zn_{0.1}Zr_{0.1}O_{3-\delta}$	*Pm-3m*	100	3.9413(1)	-	61.224(2)	5.5322	2.06	2.92
$SrFe_{0.525}Mo_{0.175}Zn_{0.15}Zr_{0.15}O_{3-\delta}$	*Pm-3m*	100	3.9579(1)	-	61.999(1)	5.4964	2.15	3.09
$SrFe_{0.45}Mo_{0.15}Zn_{0.2}Zr_{0.2}O_{3-\delta}$	*Pm-3m* *I4/mmm*	97.7 2.3	3.9746(1) 3.966(8)	- 20.125(5)	62.791(3) 316.5(1)	5.4600 5.4719	2.47	3.59

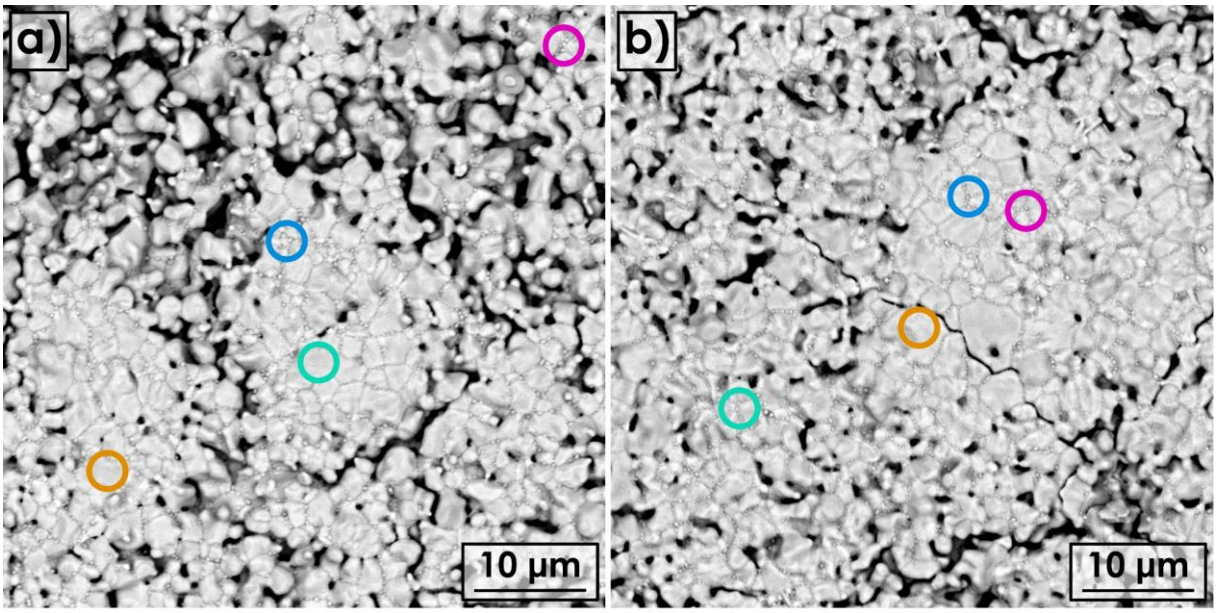

	Sr	Fe	Mo	Zn	Zr	O
○	29.7	16.6	6.8	0.5	1.7	44.7
○	25.4	38.6	3.4	0.0	0.5	32.1
○	26.4	12.5	5.9	0.5	1.5	53.2
○	25.3	11.7	5.8	0.3	2.1	54.8

	Sr	Fe	Mo	Zn	Zr	O
○	27.2	14.4	5.2	0.2	3.1	49.9
○	29.0	14.7	5.3	0.8	2.7	47.5
○	29.2	15.3	5.4	0.3	2.9	46.9
○	21.6	10.6	4.2	0.2	2.4	61.0

Figure S6. SEM micrographs with corresponding point analysis from EDS method for: a) $SrFe_{0.675}Mo_{0.225}Zn_{0.05}Zr_{0.05}O_{3-\delta}$ and b) $SrFe_{0.6}Mo_{0.2}Zn_{0.1}Zr_{0.1}O_{3-\delta}$ pellets annealed under reducing conditions (800 °C, 20 h, 10% vol. H_2 in Ar).

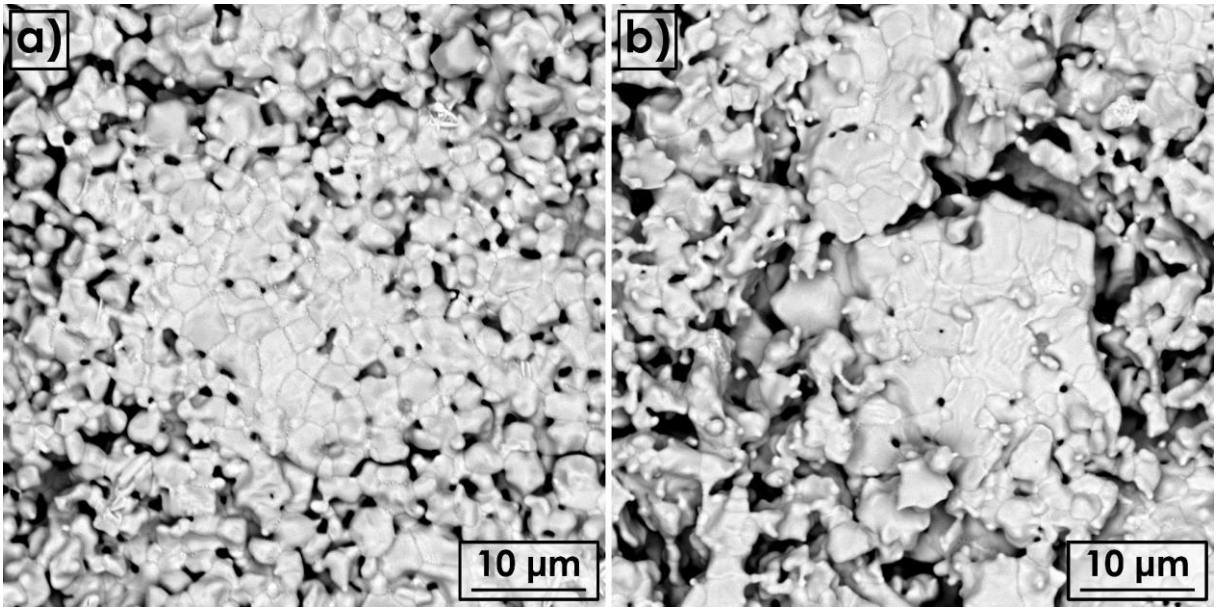

Figure S7. SEM micrographs for a) $SrFe_{0.525}Mo_{0.175}Zn_{0.15}Zr_{0.15}O_{3-\delta}$ and b) $SrFe_{0.45}Mo_{0.15}Zn_{0.2}Zr_{0.2}O_{3-\delta}$ pellets annealed under reducing conditions (800 °C, 20 h, 10% vol. H_2 in Ar).

Supplementary Note 1

To provide deeper insight into the reduction behavior and its implications in terms of valency of individual ions, the XPS studies were conducted for $SrFe_{0.6}Mo_{0.2}Zn_{0.1}Zr_{0.1}O_{3-\delta}$, as the $x = 0.1$ material appears to be a transition point for a number of the structural features. Both the as-sintered material, and the one subjected to prior treatment under reducing conditions were investigated, with results presented in Figure S9. The data for the pre-sputtered samples can be found in Figure S10. However, due to visible interference of the measurement with the valence state of the ions, they were not considered for further analysis. Nevertheless, the results for the pre-sputtered samples can be used as a reference point for the spectra of non-redox elements, such as Sr^{2+}, Zn^{2+}, and Zr^{4+}, under pristine conditions, as even for the zirconium, the reduction is practically impossible under studied conditions.

The as-sintered $SrFe_{0.6}Mo_{0.2}Zn_{0.1}Zr_{0.1}O_{3-\delta}$ material displays characteristics that are consistent with the typical SFM material. According to thermodynamic data [1], under oxidizing conditions, the ionic configuration of conventional $SrFe_{0.75}Mo_{0.25}O_{3-\delta}$ is dominated by Mo^{6+} and Fe^{3+} ions, as the content of minority Mo^{5+} and Fe^{2+} is orders of magnitude lower, which appears to be the case in Figure S9 [2,3]. Although for Fe the analysis of the valence states is particularly challenging due to the common presence of multiplet splitting, and therefore unambiguous assignment of the individual peaks in our opinion is not possible, the position of last shake-up line found at 718.2 eV, clearly indicates the prevailing content of Fe^{3+} in high-spin configuration [3]. Interestingly, the behavior under reducing conditions is remarkably similar, with a preserved dominant content of Mo^{6+} and Fe^{3+} ions, although the molybdenum peaks are slightly shifted toward lower energies, possibly indicating slight lowering of the effective charge. In the case of conventional SFM, the content of Mo^{5+} becomes comparable to Mo^{6+} only at oxygen partial pressure in the vicinity of 10^{-15} to 10^{-20} bars (depending on the temperature) [1], while for Fe^{2+} its content even under reducing conditions remains an order of magnitude lower than Fe^{3+}, which, taking into account the use of 10% H_2 in Ar in our study, points to a very similar behavior of doped materials. As the XPS measurements were conducted on the cleaved surface, the lack of metallic Fe signal likely points to the surface character of the exsolved nanoprecipitates. Finally, worth noting is that under both oxidizing and reducing conditions, the behavior of Sr and Zr appears not to be as straightforward as could be expected, with multiple shifts in their peaks positions. Based on the comparison with the spectra for pre-sputtered samples and literature [4,5], these changes indicate that despite all precautions, the studied surface of the cleaved un-

sputtered samples may have a small level of contamination, or that reconstruction of the surface took place.

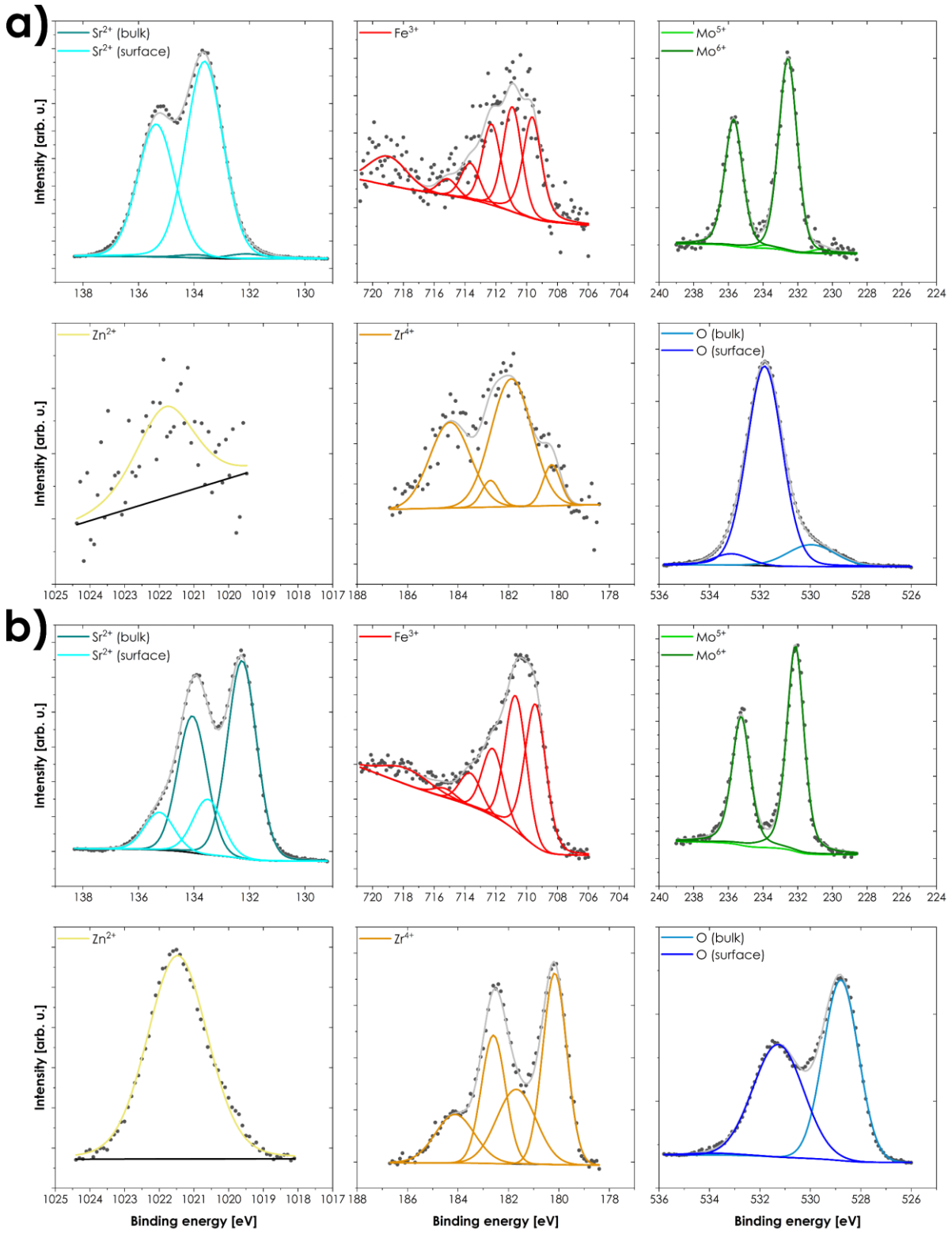

Figure S8. XPS spectra collected for $SrFe_{0.6}Mo_{0.2}Zn_{0.1}Zr_{0.1}O_{3-\delta}$ (without prior ion sputtering): a) sample annealed for 20 h at 1200 °C in air; b) sample additionally annealed in 10% H_2 in Ar at 800 °C for 24 h. In each case the experimental points are marked by dark grey dots, composite spectrum as a light grey line, and background as a black line.

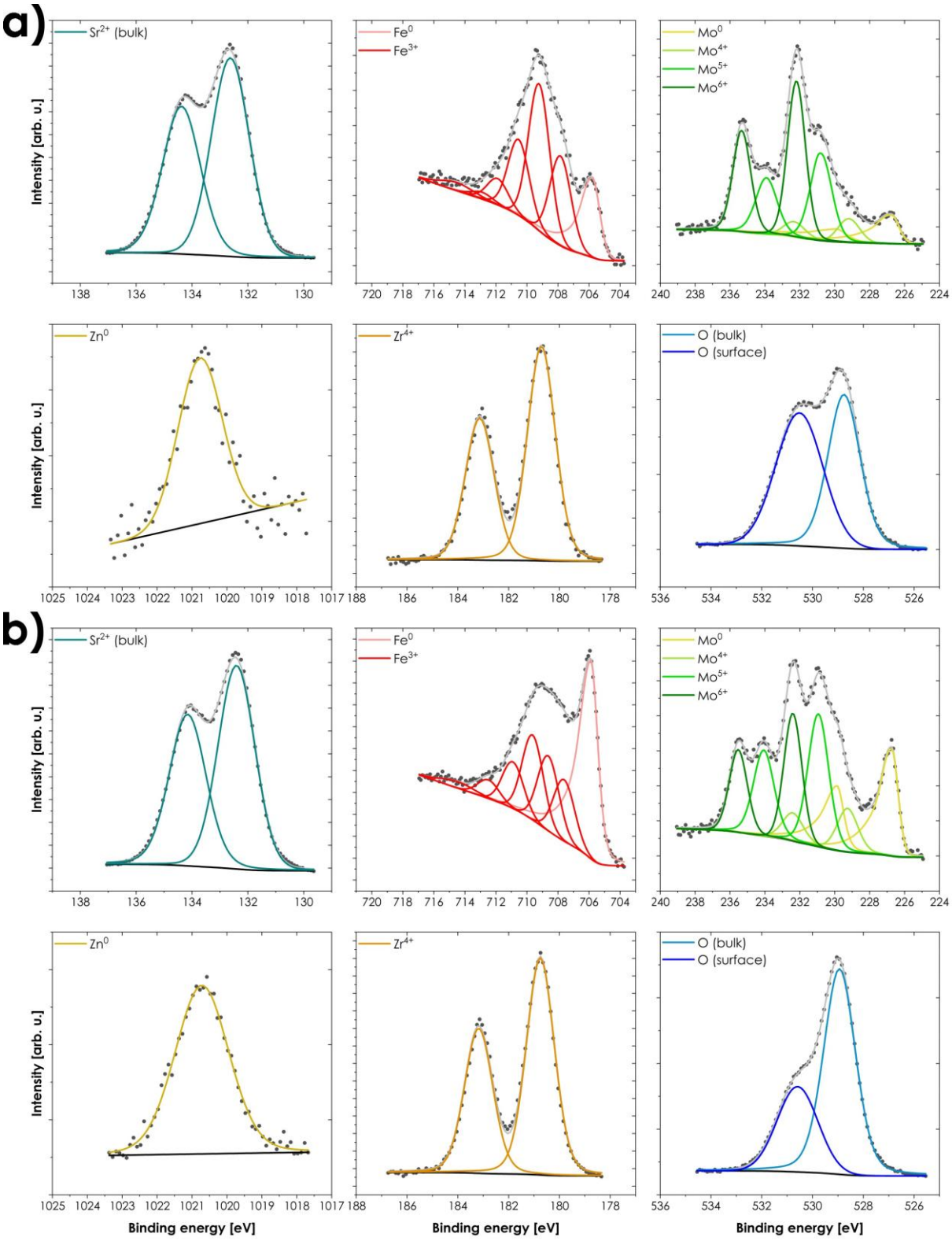

Figure S9. XPS spectra collected for $SrFe_{0.6}Mo_{0.2}Zn_{0.1}Zr_{0.1}O_{3-\delta}$ (with prior ion sputtering): a) sample annealed for 20 h at 1200 °C in air; b) sample additionally annealed in 10% H_2 in Ar at 800°C for 24 h. In each case the spectrum is presented as dark grey dots, composite spectrum as a light grey line, and background as a black line.

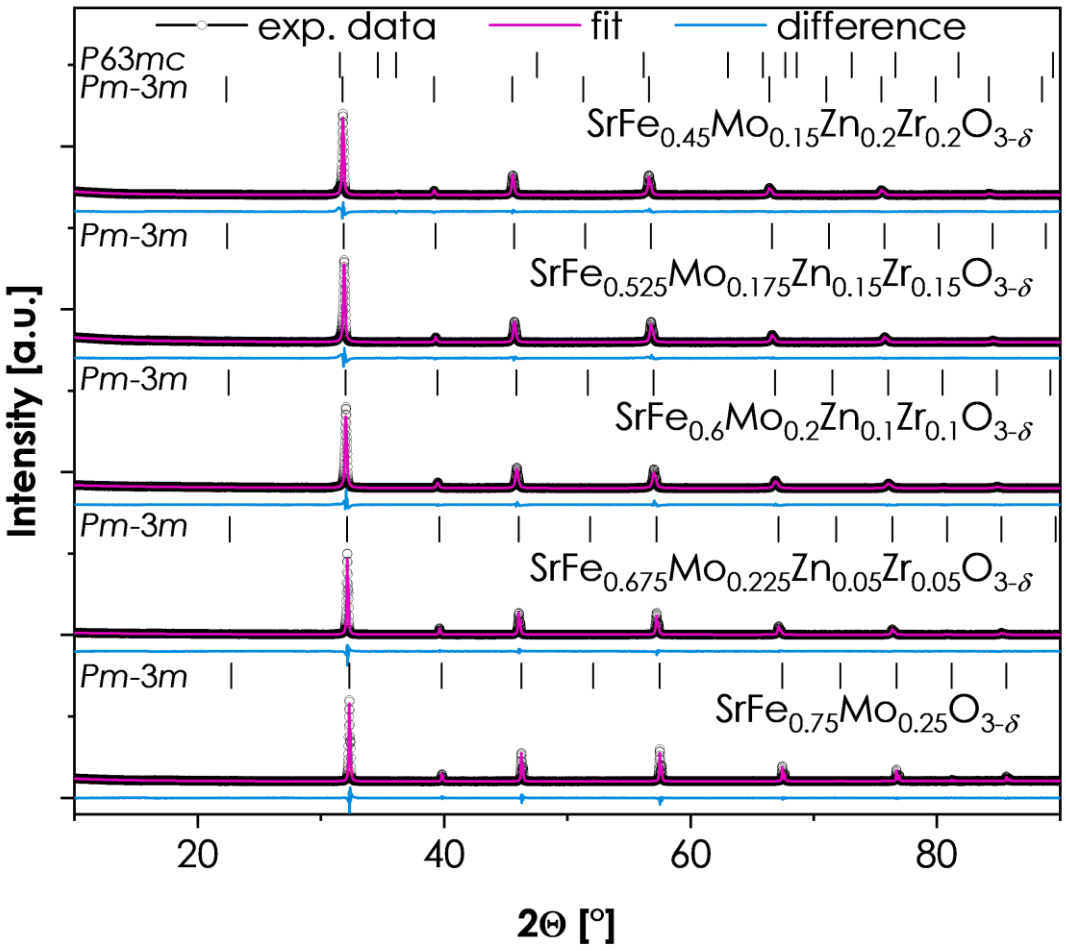

Figure S10. X-ray diffractograms for $Sr(Fe_{0.75}Mo_{0.25})_{1-2x}Zn_xZr_xO_{3-\delta}$ (x = 0, 0.05, 0.1, 0.15 and 0.2) materials after annealing at 900 °C for 6 hours, in atmosphere of 5% H_2/Ar mixture, together with the results of Rietveld refinement.

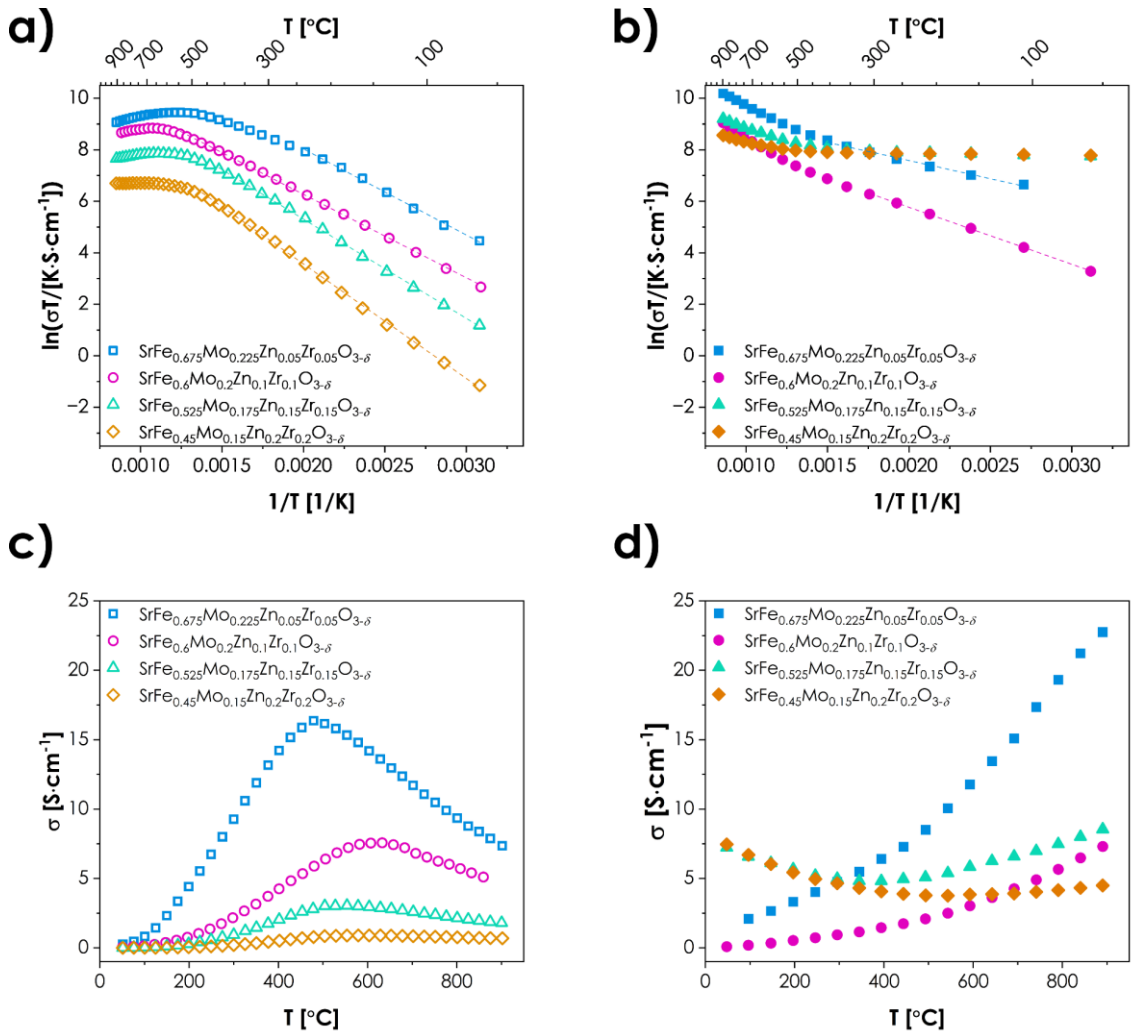

Figure S11. Arrhenius plots together with linear fitting for the $Sr(Fe_{0.75}Mo_{0.25})_{1-2x}Zn_xZr_xO_{3-\delta}$ (x = 0.05, 0.1, 0.15, and 0.2) a) in air; b) under reducing conditions. Temperature dependence of electrical conductivity values for the $Sr(Fe_{0.75}Mo_{0.25})_{1-2x}Zn_xZr_xO_{3-\delta}$ (x = 0.05, 0.1, 0.15, and 0.2) c) in air; d) under reducing conditions.

Table S3. The results of Rietveld refinement for $Sr(Fe_{0.75}Mo_{0.25})_{1-2x}Zn_xZr_xO_{3-\delta}$ (x = 0, 0.05, 0.1, 0.15, and 0.2) materials with: GDC and LSGM, after sintering at 1100 °C for 2 h.

Composition	Space group	Content (wt. %)	*a* [Å]	*V* [Å^3]	GoF [-]	Rwp [%]
$SrFe_{0.675}Mo_{0.225}Zn_{0.05}Zr_{0.05}O_{3-\delta}$ + GDC	*Pm*-3*m*	77.5	3.9292(1)	60.662(1)	1.63	3.28
	Fm-3*m*	22.5	5.4236(1)	159.536(3)		
$SrFe_{0.6}Mo_{0.2}Zn_{0.1}Zr_{0.1}O_{3-\delta}$ + GDC	*Pm*-3*m*	78.6	3.9414(1)	61.230(2)	1.81	3.72
	Fm-3*m*	21.4	5.4236(1)	159.539(5)		
$SrFe_{0.525}Mo_{0.175}Zn_{0.15}Zr_{0.15}O_{3-\delta}$ + GDC	*Pm*-3*m*	79.8	3.9544(1)	61.836(2)	1.89	3.96
	Fm-3*m*	20.2	5.4234(1)	159.521(5)		
$SrFe_{0.45}Mo_{0.15}Zn_{0.2}Zr_{0.2}O_{3-\delta}$ + GDC	*Pm*-3*m*	79.2	3.9684(1)	62.496(2)	2.01	4.25
	Fm-3*m*	20.8	5.4233(1)	159.508(6)		
$SrFe_{0.675}Mo_{0.225}Zn_{0.05}Zr_{0.05}O_{3-\delta}$ + LSGM	*Pm*-3*m*	83.5	3.9290(1)	60.654(1)	1.36	2.68
	Pm-3*m*	15.2	3.9137(1)	59.946(2)		
	I4/mmm	1.3	3.8554(5)	189.41(4)		
$SrFe_{0.6}Mo_{0.2}Zn_{0.1}Zr_{0.1}O_{3-\delta}$ + LSGM	*Pm*-3*m*	83.1	3.9407(1)	61.194(2)	1.50	2.98
	Pm-3*m*	13.7	3.9135(1)	59.939(2)		
	I4/mmm	3.2	3.8556(4)	189.52(3)		
$SrFe_{0.525}Mo_{0.175}Zn_{0.15}Zr_{0.15}O_{3-\delta}$ + LSGM	*Pm*-3*m*	82.0	3.9538(1)	61.807(1)	1.50	2.97
	Pm-3*m*	12.1	3.9135(1)	59.939(2)		
	I4/mmm	5.9	3.8564(2)	189.50(2)		
$SrFe_{0.45}Mo_{0.15}Zn_{0.2}Zr_{0.2}O_{3-\delta}$ + LSGM	*Pm*-3*m*	79.8	3.9680(1)	62.476(2)	1.79	3.73
	Pm-3*m*	11.4	3.9133(1)	59.927(3)		
	I4/mmm	8.8	3.8557(2)	189.43(2)		

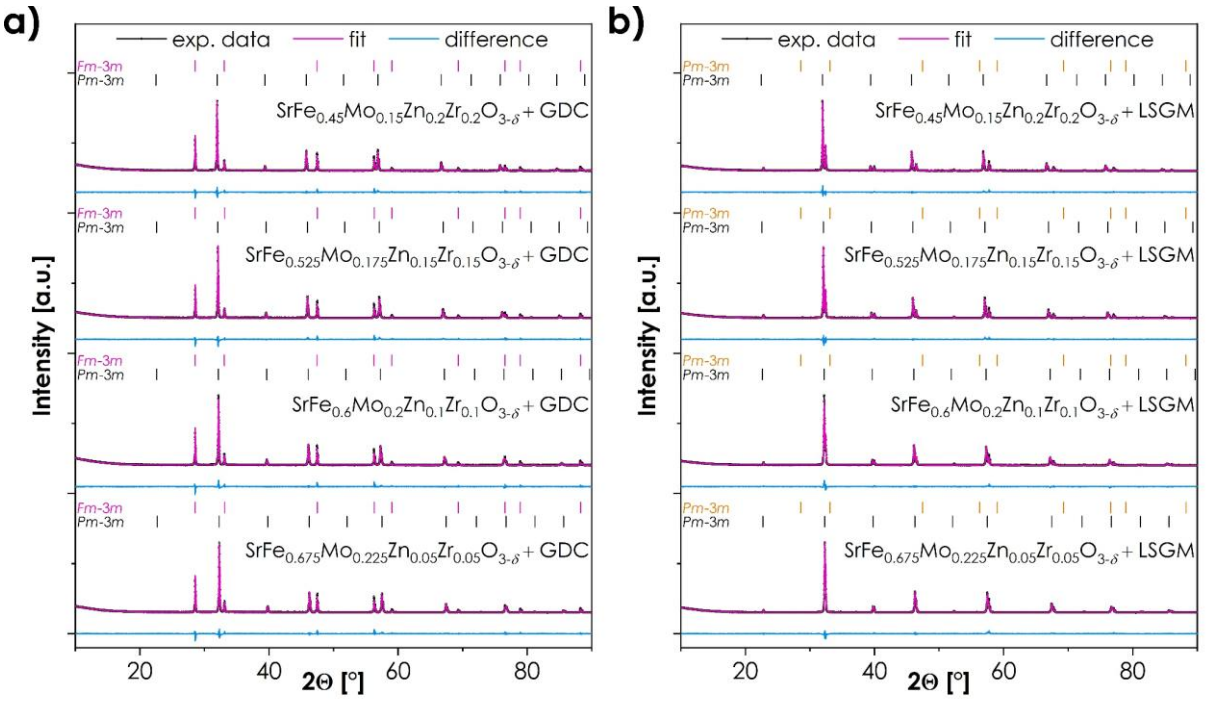

Figure S12. XRD diffractograms for mixtures of each material with: a) GDC; b) LSGM, after sintering at 800 °C for 100 h.

Table S4. The results of Rietveld refinement for $Sr(Fe_{0.75}Mo_{0.25})_{1-2x}Zn_xZr_xO_{3-\delta}$ (x = 0, 0.05, 0.1, 0.15, and 0.2) materials with: GDC and LSGM, after sintering at 800 °C for 100 h.

Composition	Space group	Content (wt. %)	a [Å]	V [Å^3]	GoF [-]	Rwp [%]
$SrFe_{0.675}Mo_{0.225}Zn_{0.05}Zr_{0.05}O_{3-\delta}$	*Pm*-3*m*	80.5	3.9289(1)	60.647(1)	1.72	3.43
+ GDC	*Fm*-3*m*	19.5	5.4235(1)	159.533(5)		
$SrFe_{0.6}Mo_{0.2}Zn_{0.1}Zr_{0.1}O_{3-\delta}$	*Pm*-3*m*	80.1	3.9410(1)	61.209(2)	1.74	3.53
+ GDC	*Fm*-3*m*	19.9	5.4236(1)	159.534(5)		
$SrFe_{0.525}Mo_{0.175}Zn_{0.15}Zr_{0.15}O_{3-\delta}$	*Pm*-3*m*	81.6	3.9537(1)	61.804(1)	1.75	3.60
+ GDC	*Fm*-3*m*	18.4	5.4235(1)	159.533(5)		
$SrFe_{0.45}Mo_{0.15}Zn_{0.2}Zr_{0.2}O_{3-\delta}$	*Pm*-3*m*	79.0	3.9680(1)	62.477(1)	1.63	3.44
+ GDC	*Fm*-3*m*	21.0	5.4236(1)	159.536(4)		
$SrFe_{0.675}Mo_{0.225}Zn_{0.05}Zr_{0.05}O_{3-\delta}$	*Pm*-3*m*	86.4	3.9288(1)	60.641(1)	1.50	2.98
+ LSGM	*Pm*-3*m*	13.6	3.9136(1)	59.940(2)		
$SrFe_{0.6}Mo_{0.2}Zn_{0.1}Zr_{0.1}O_{3-\delta}$	*Pm*-3*m*	84.1	3.9410(1)	61.208(1)	1.56	2.98
+ LSGM	*Pm*-3*m*	15.9	3.9138(1)	59.952(2)		
$SrFe_{0.525}Mo_{0.175}Zn_{0.15}Zr_{0.15}O_{3-\delta}$	*Pm*-3*m*	82.8	3.9540(1)	61.819(1)	1.43	2.88
+ LSGM	*Pm*-3*m*	17.2	3.9137(1)	59.948(1)		
$SrFe_{0.45}Mo_{0.15}Zn_{0.2}Zr_{0.2}O_{3-\delta}$	*Pm*-3*m*	81.3	3.9686(1)	62.504(1)	1.63	3.44
+ LSGM	*Pm*-3*m*	18.7	3.9136(1)	59.943(1)		

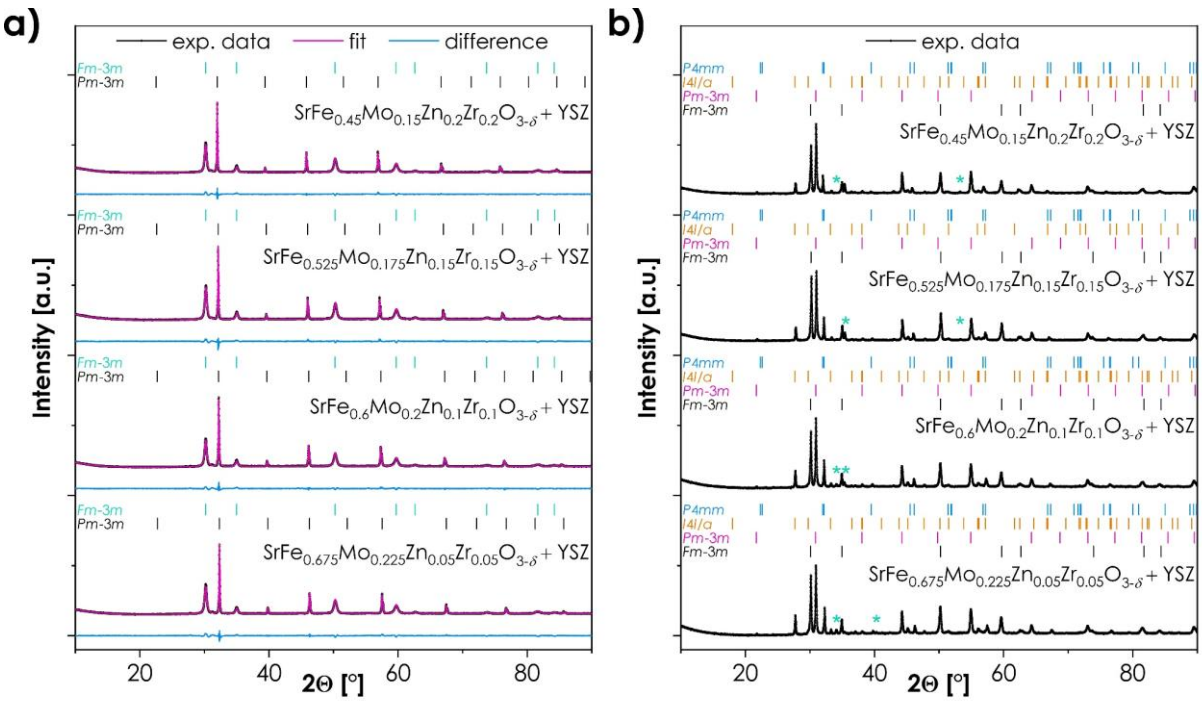

Figure S13. X-ray diffractograms for mixtures of each material with YSZ after sintering: a) at 800 °C for 100 h; b) at 1100 °C for 2 h.

Table S5. The results of Rietveld refinement for $Sr(Fe_{0.75}Mo_{0.25})_{1-2x}Zn_xZr_xO_{3-\delta}$ (x = 0, 0.05, 0.1, 0.15, and 0.2) materials with YSZ, after sintering at 800 °C for 100 h.

Composition	Space group	Content (wt. %)	*a* [Å]	*V* [Å^3]	GoF [-]	Rwp [%]
$SrFe_{0.675}Mo_{0.225}Zn_{0.05}Zr_{0.05}O_{3-\delta}$	*Pm*-3*m*	44.7	3.9284(1)	60.622(2)	1.62	2.63
+ YSZ	*Fm*-3*m*	55.3	5.1423(1)	135.98(1)		
$SrFe_{0.6}Mo_{0.2}Zn_{0.1}Zr_{0.1}O_{3-\delta}$	*Pm*-3*m*	45.9	3.9402(1)	61.171(2)	1.61	2.66
+ YSZ	*Fm*-3*m*	54.1	5.1423(1)	135.98(1)		
$SrFe_{0.525}Mo_{0.175}Zn_{0.15}Zr_{0.15}O_{3-\delta}$	*Pm*-3*m*	40.9	3.9535(1)	61.794(2)	1.61	2.74
+ YSZ	*Fm*-3*m*	59.1	5.1420(1)	135.954(9)		
$SrFe_{0.45}Mo_{0.15}Zn_{0.2}Zr_{0.2}O_{3-\delta}$	*Pm*-3*m*	42.2	3.9684(1)	62.496(2)	1.65	2.77
+ YSZ	*Fm*-3*m*	57.3	5.1423(1)	135.980(8)		

Supplementary Note 2

As can be seen, three materials from the series, $SrFe_{0.675}Mo_{0.225}Zn_{0.05}Zr_{0.05}O_{3-\delta}$, $SrFe_{0.6}Mo_{0.2}Zn_{0.1}Zr_{0.1}O_{3-\delta}$, and $SrFe_{0.525}Mo_{0.175}Zn_{0.15}Zr_{0.15}O_{3-\delta}$, are stable toward the GDC electrolyte under conditions corresponding to cell fabrication. However, the material with the highest dopant content, $SrFe_{0.45}Mo_{0.15}Zn_{0.2}Zr_{0.2}O_{3-\delta}$, exhibits a considerable level of instability, and therefore is not considered in further evaluation (see Figure S11 and Table S3). Furthermore, all materials were found to be unstable toward the LSGM and YSZ electrolytes after sintering at 1100 °C for 2 h (see Figure S12-S13 and Table S4-S5). On the other hand, no signs of reactivity can be seen for all the combinations of cathodes/electrolytes under conditions corresponding to cell operation. Combined with the relatively small changes in the lattice parameters, compared to the base materials, it might indicate the possibility of using different types of electrolytes in the future, after adjusting the processing conditions of the cathode layer. Nevertheless, on the basis of the presented results, the GDC electrolyte was selected for the preparation of symmetric cells.

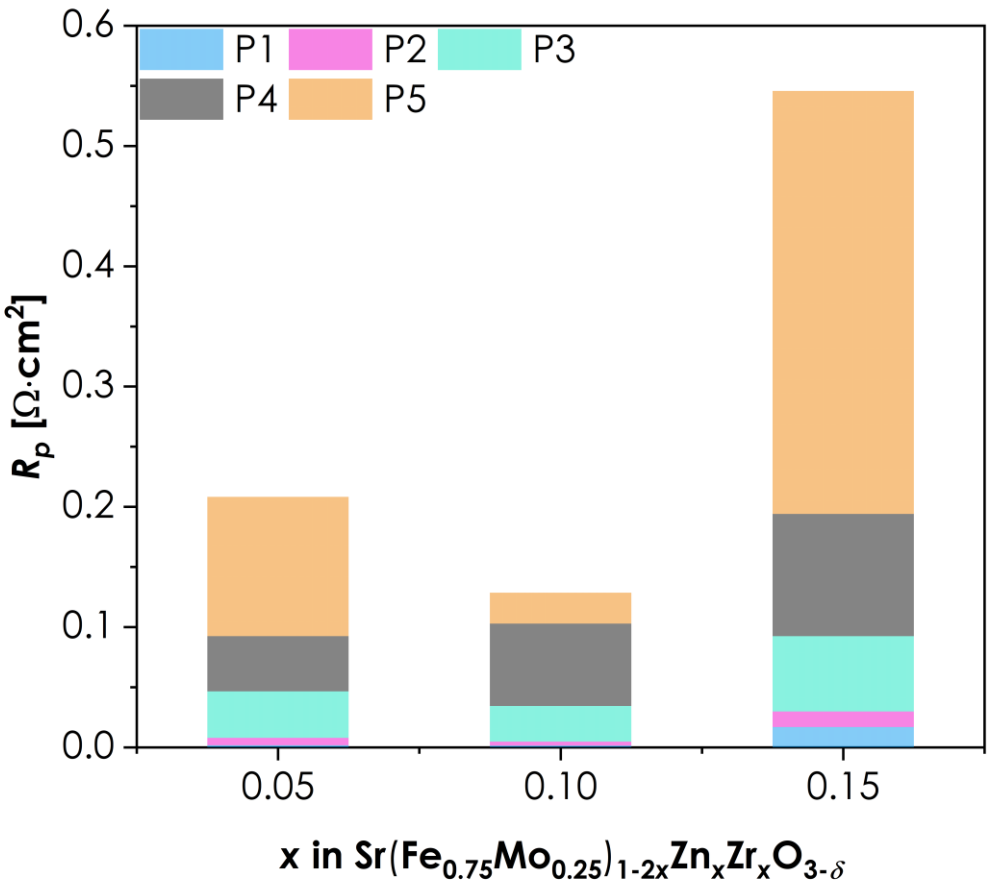

Figure S14. Comparison of the contribution of cathodic processes to the total polarization resistance.

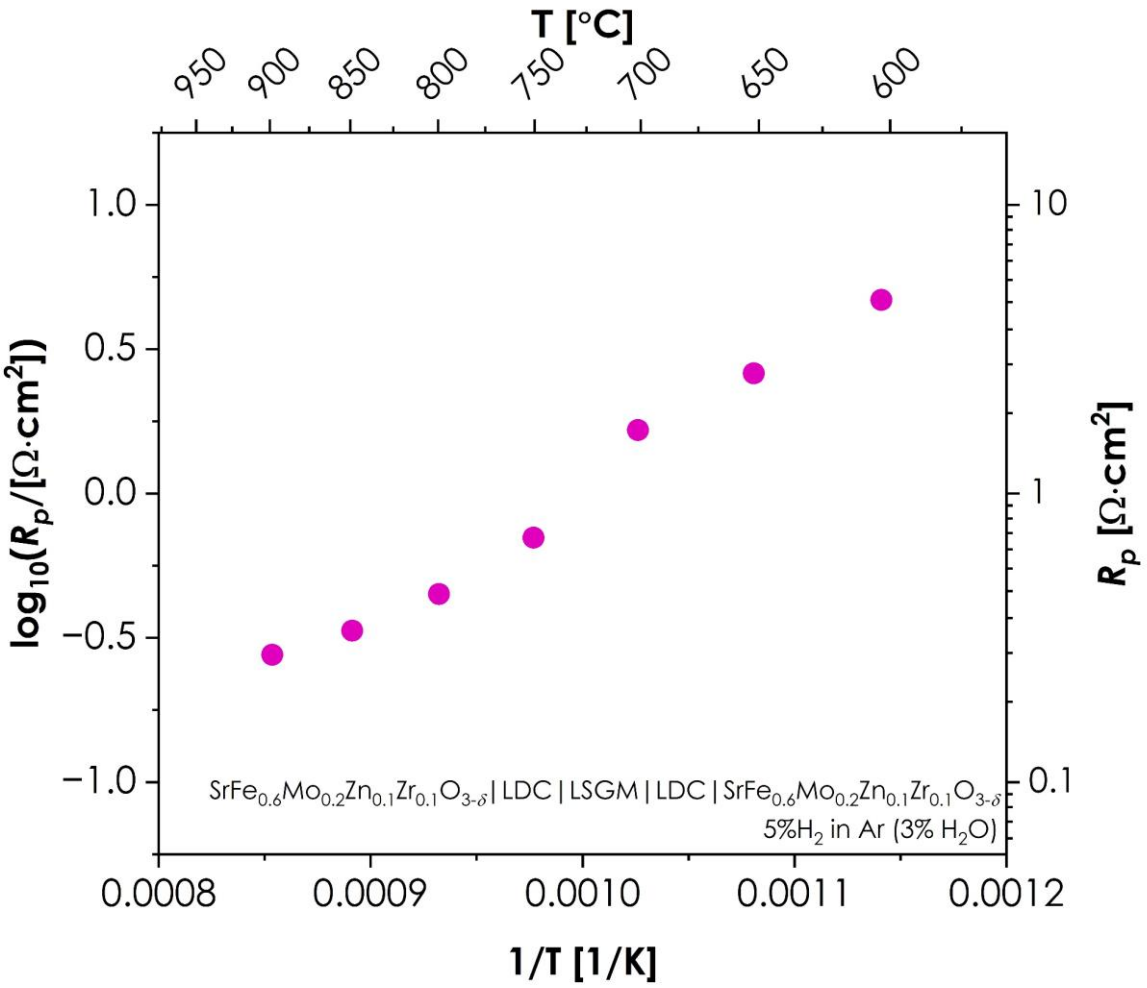

Figure S15. Anodic polarization resistance values for $SrFe_{0.6}Mo_{0.2}Zn_{0.1}Zr_{0.1}O_{3-\delta}$ material as a function of temperature measured under 5% H_2 in Ar (3% H_2O) atmosphere.

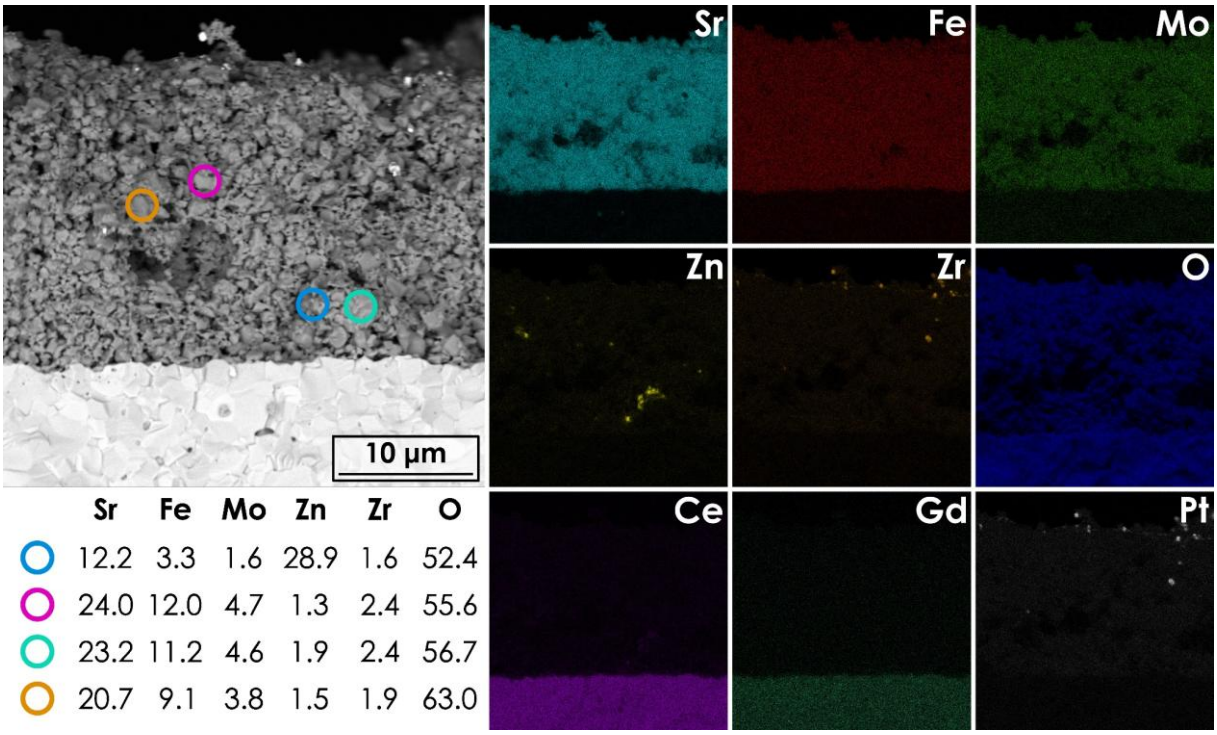

	Sr	Fe	Mo	Zn	Zr	O
○	12.2	3.3	1.6	28.9	1.6	52.4
○	24.0	12.0	4.7	1.3	2.4	55.6
○	23.2	11.2	4.6	1.9	2.4	56.7
○	20.7	9.1	3.8	1.5	1.9	63.0

Figure S16. Cross-section of $SrFe_{0.6}Mo_{0.2}Zn_{0.1}Zr_{0.1}O_{3-\delta}$|GDC|$SrFe_{0.6}Mo_{0.2}Zn_{0.1}Zr_{0.1}O_{3-\delta}$ symmetrical cell with Pt current collector. The cell was subjected to polarization resistance temperature-dependent (600 – 800 °C) measurements beforehand. Noteworthy, the signal from the Pt collector overlaps to some degree with Zr one.

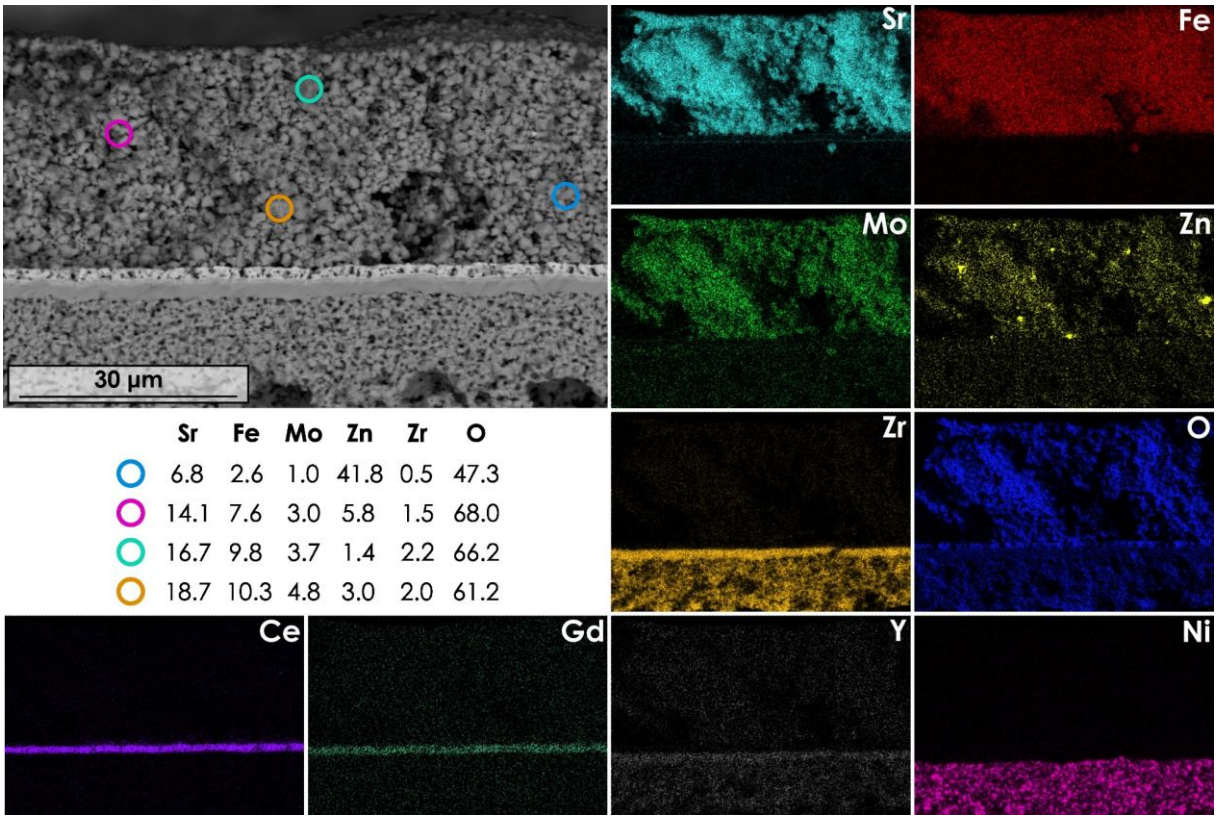

Figure S17. Cross-section of $SrFe_{0.6}Mo_{0.2}Zn_{0.1}Zr_{0.1}O_{3-\delta}$|GDC|YSZ|Ni+YSZ full cell. The cell was tested in the 600 – 900 °C range measurements beforehand.

References

(1) Merkulov, O. V.; Naumovich, E. N.; Patrakeev, M. V.; Markov, A. A.; Bouwmeester, H. J. M.; Leonidov, I. A.; Kozhevnikov, V. L. Oxygen Nonstoichiometry and Defect Chemistry of Perovskite-Structured $SrFe_{1-x}Mo_xO_{3-\delta}$ Solid Solutions. *Solid State Ionics* **2016**, *292*, 116–121. https://doi.org/10.1016/j.ssi.2016.05.009.

(2) Baltrusaitis, J.; Mendoza-Sanchez, B.; Fernandez, V.; Veenstra, R.; Dukstiene, N.; Roberts, A.; Fairley, N. Generalized Molybdenum Oxide Surface Chemical State XPS Determination via Informed Amorphous Sample Model. *Applied Surface Science* **2015**, *326*, 151–161. https://doi.org/10.1016/j.apsusc.2014.11.077.

(3) Grosvenor, A. P.; Kobe, B. A.; Biesinger, M. C.; McIntyre, N. S. Investigation of Multiplet Splitting of Fe 2p XPS Spectra and Bonding in Iron Compounds. *Surface & Interface Analysis* **2004**, *36* (12), 1564–1574. https://doi.org/10.1002/sia.1984.

(4) Mueller, D. N.; Machala, M. L.; Bluhm, H.; Chueh, W. C. Redox Activity of Surface Oxygen Anions in Oxygen-Deficient Perovskite Oxides during Electrochemical Reactions. *Nat Commun* **2015**, *6* (1), 6097. https://doi.org/10.1038/ncomms7097.

(5) Anderson, J. A.; Fierro, J. L. G. Bulk and Surface Properties of Copper-Containing Oxides of the General Formula $LaZr_{1-x}Cu_xO_3$. *Journal of Solid State Chemistry* **1994**, *108* (2), 305–313. https://doi.org/10.1006/jssc.1994.1047.